Published in final edited form as:
Ultrasound Med Biol. 2012 June ; 38(6): 1019–1029. doi:10.1016/j.ultrasmedbio.2012.01.014.

Contrast Ultrasound Imaging for Identification of Early Responder Tumor Models to Anti-Angiogenic Therapy

Shashank Sirsi[1,2], **Molly Flexman**[3], **Fotis Vlachos**[3], **Jianzhong Huang**[4], **Sonia L. Hernandez**[5], **Hyun Keol Kim**[3], **Tessa J. Johung**[4], **Jeffrey Gander**[4], **Ari Reichstein**[4], **Brooke S. Lampl**[6], **Antai Wang**[7], **Andreas H. Hielscher**[3,6,8], **Jessica J. Kandel**[3,9], **Darrell J. Yamashiro**[4,5,9], and **Mark Borden**[1,2,9]

[1]Department of Chemical Engineering, Columbia University, New York, NY 10027

[2]Department of Mechanical Engineering, University of Colorado, Boulder, CO 80309

[3]Department of Biomedical Engineering, Columbia University, New York, NY 10027

[4]Department of Surgery, Columbia University, New York, NY 10032

[5]Department of Pediatrics and Pathology, Columbia University, New York, NY 10032

[6]Department of Radiology, Columbia University, New York, NY 10032

[7]Department of Biostatistics, Columbia University, New York, NY 10032

[8]Department of Electrical Engineering, Columbia University, New York, NY 10027

Abstract

Agents targeting vascular endothelial growth factor (VEGF) have been validated as cancer therapeutics, yet efficacy can differ widely between tumor types and individual patients. In addition, such agents are costly and can have significant toxicities. Rapid noninvasive determination of response could provide significant benefits. We tested if response to the anti-VEGF antibody bevacizumab (BV) could be detected using contrast-enhanced ultrasound imaging (CEUS). We used two xenograft model systems with previously well-characterized responses to VEGF inhibition, a responder (SK-NEP-1) and a non-responder (NGP), and examined perfusion-related parameters. CEUS demonstrated that BV treatment arrested the increase in blood volume in the SK-NEP-1 tumor group only. Molecular imaging of $\alpha_V\beta_3$ with targeted microbubbles was a more sensitive prognostic indicator of BV efficacy. CEUS using RGD-labeled microbubbles showed a robust decrease in $\alpha_V\beta_3$ vasculature following BV treatment in SK-NEP-1 tumors. Paralleling these findings, lectin perfusion assays detected a disproportionate pruning of smaller, branch vessels. Therefore, we conclude that the response to BV can be identified soon after initiation of treatment, often within 3 days, by use of CEUS molecular imaging techniques. The use of a noninvasive ultrasound approach may allow for earlier and more effective determination of efficacy of anti-angiogenic therapy.

*Corresponding Author Address: Mark Borden, Department of Mechanical Engineering, University of Colorado at Boulder, 1111 Engineering Drive, 427 UCB, Boulder, CO 80309, Phone: (303) 492-7750, mark.borden@colorado.edu.
[9]These senior authors contributed equally to this work

Keywords

bevacizumab; VEGF blockade; Wilms tumor; neuroblastoma; molecular imaging; blood volume; microbubble

Introduction

The emergence of treatments that target specific biological processes in tumors, such as blood vessel development, has been only modestly successful overall, yet highly effective in subsets of patients. This variability, combined with the potential adverse effects and high cost of these novel treatments, suggests that a rapid noninvasive means of benchmarking tumor responses would be useful. In this work, we used contrast-enhanced ultrasound (CEUS) to monitor immediate tumor vascular changes in response to anti-VEGF therapy. Ultrasound contrast agents were used to measure the relative tumor blood volumes and levels of angiogenic activity in two tumor types known to be responsive or non-responsive to VEGF blockade therapy. Two quantitative CEUS techniques were compared to histological analysis of tissue with the goal of identifying the most accurate prognostic method of clearly distinguishing responder from non-responder tumor types within a short time after commencement of treatment.

While ultrasound has been used in clinical settings for over 40 years, recent technological advances have opened the doors to many new applications. The high compressibility and resonance behavior of gas-filled microbubbles makes them useful intravascular ultrasound contrast agents, allowing their acoustic signal to be readily differentiated from tissue. Contrast detection modes are already available on several clinical ultrasound scanners. CEUS provides real-time imaging at the bedside for qualitative tracking and quantitative measurement of perfusion-related biomarkers (Feshitan, Chen 2009, Williams, Hudson 2011). CEUS is currently used to assess malignancy of liver, bowel, kidney, pancreas, breast and prostate lesions by measuring perfusion-related parameters, such as uptake and washout of contrast (Wilson and Burns 2010, Wilson, Greenbaum 2009). Additionally, CEUS has been used to illustrate the response of tumor models to VEGF blockade (Cheung, Brown 2007, Forsberg, Ro 2004, Guibal, Taillade 2010, Hoyt, Warram), but few studies have focused on differentiating responder from non-responder neoplasms. CEUS also has been used in clinical pilot studies to predict improvement in progression-free and overall survival of patients with renal cell carcinoma treated with sorafenib (Nexavar) (Lamuraglia, Escudier 2006), as well as predicting gastrointestinal tumor responses to imatinib (Glivec) therapy (Lassau, Lamuraglia 2006). However, these prior studies did not utilize targeted microbubbles for molecular imaging to distinguish cohorts of responder and non-responder tumors.

In these studies, we used two tumor models with previously extensively characterized and divergent responses to vascular endothelial growth factor (VEGF) inhibition. Xenografts from the SK-NEP-1 human Ewing family tumor cell line (Smith, Morton 2008), are highly responsive to various anti-VEGF agents, with significant loss of vasculature and inhibition of growth. In contrast, xenografts from the NGP human neuroblastoma cell line continue to grow with only slight restriction and minimally destabilized vessels (Huang, Frischer 2003, Kim, Serur 2002, Rowe, Huang 2000, Rowe, Huang 2000). We asked, using CEUS, whether differences in microbubble signal enhancement could differentiate between the responder (SK-NEP-1) and non-responder (NGP) tumor models, and whether such changes could be detected early after the start of treatment with the anti-VEGF antibody bevacizumab (BV). Our findings suggest that a noninvasive ultrasound imaging strategy can provide a rapid

readout of tumor responsiveness to VEGF inhibition between cohorts of tumor-bearing mice, which may be extended to allow for tailoring therapy for individual patients.

Methods

Microbubble Formulation and Peptide Conjugation

Lipid-coated microbubbles used in this study were produced by a shaking method (Unger, Lund 1992). In our procedure, a lipid stock solution containing 90 mol% 1,2-distearyol-sn-glycero-3-phosphocholine (DSPC), 5 mol% 1,2-distearyol-sn-glycero-3-phosphoethanolamine-N-[methoxy(polyethylene glycol)2000] (DSPE-PEG2000) and 5 mol % 1,2-distearyol-sn-glycero-3-phosphoethanolamine-N-[maleimide(polyethylene glycol)2000] (DSPE-PEG2000-Maleimide), purchased from Avanti Polar Lipids (Alabaster, AL), was made in 150 mM NaCl phosphate buffered saline (PBS) pH 7.4 at 1 mg/mL of total lipid. 2 mL of the lipid solution was warmed to 60 °C in a sealed 3-mL glass serum vial (Wheaton, Millville, NJ) and briefly bath sonicated to disperse the lipid. The air headspace was exchanged with perfluorobutane gas (PFB) obtained from FluoroMed (Round Rock, TX) using a custom gas exchange apparatus. The pressure in the vial was vented to the atmosphere, and the microbubbles were formed by rapidly shaking the vial for 45 seconds using a VialMix shaker (Bristol-Myers Squibb, New York City, NY). Five vials were prepared and the microbubble suspensions were pooled.

Lipid vesicles and microbubbles less than 2 μm diameter were removed using methods previously described (Feshitan, Chen 2009, Sirsi, Feshitan 2010). Our previous research has demonstrated that small microbubbles (<2 μm diameter) are poor contrast agents for high-frequency fundamental mode imaging (40 MHz) (Sirsi, Feshitan 2010). Larger microbubbles (>3 μm diameter) demonstrated greater signal enhancement and longer circulation times. Previous research has also demonstrated that size-selected microbubbles (mean diameter of 3.3 μm) produce approximately a 20-fold signal enhancement compared the non-size selected bubbles (mean diameter of 0.9 μm) for molecular imaging using a clinical ultrasound scanner (Streeter, Gessner 2010). Therefore, microbubbles smaller than 2 μm were removed from suspension for this study. Microbubble size-selection was performed by differential centrifugation (Feshitan, Chen 2009, Sirsi, Feshitan 2010). Briefly, the microbubble suspension was repeatedly centrifuged at 90 relative centrifugal force (RCF) for 1 minute using a bucket-rotor centrifuge (Model 5804, Eppendorf, Westbury, NY) to remove bubbles less than 2 μm. The final microbubble cake was resuspended in 2 mL of PBS (pH 6.5; 5 mM EDTA). The concentration and size distribution of the resulting suspension were evaluated using an Accusizer 280A (NICOMP Particle Sizing Systems, Santa Barbara, CA).

All microbubbles were labeled with cysteine-modified cyclic RGD or RAD peptides (Peptides International, Louisville, Kentucky). The peptides were dissolved in a degassed 3 vol%, 10 mg/mL acetic acid solution (Sigma Aldrich, St. Louis, MO) and combined with 1 mL of the size-selected microbubble suspension to a 30:1 peptide:maleimide molar ratio. The peptides were mixed with microbubbles end-over-end at 4 °C overnight to allow the thiol reactive maleimide groups on distal ends of the PEG chains (incorporated into the microbubble shell) to bind with the cysteine end-groups of the peptide. Attachment to the PEG terminus ensured that the ligands were extended beyond the polymer brush layer and exposed to the surrounding milieu. The peptide-bearing microbubbles were then concentrated by centrifugation (90 RCF for 1 minute). The resulting microbubble cake was resuspended in 0.5 mL sterile PBS (pH 7.4) and then stored until needed. Prior to injection, the microbubbles were sized and counted, then diluted to achieve 2.5×10^7 microbubbles per injection. Stability tests revealed negligible change in microbubble size or concentration

during the experiment. Microbubbles used in this study had a median diameter of 4.5 ± 0.7 μm (Fig. 1).

Preparation and Treatment of Xenograft Tumors

All animal experiments were approved by the Columbia University Institutional Animal Care and Use Committee. 10^6 cultured human SK-NEP-1 or NGP cells were implanted intrarenally in 4–6 week old female NCR nude mice as described (Huang, Frischer 2003, Kim, Serur 2002), and resulting xenografts monitored for growth using bioluminescence. At a threshold corresponding to 1–2 g, tumors were randomized to control or treatment groups (cohort size 5–8 mice per modality and treatment group, indicated in figure legends). BV 0.5 mg (2.5 mg/mL) was administered intravenously through the tail vein immediately after CEUS imaging on days 0 and 3. Albumin (2.5 mg/mL) was used as a placebo for control studies. Animals were sacrificed by CO_2 inhalation at indicated time points (at day 5 after serial imaging studies, and at days 0, 1, 3, and 5 for control and lectin perfusion analyses).

Tumor Size Progression

Our previous studies have demonstrated that xenografts formed in the kidney of NCR nude mice with the human Ewing family tumor cell line SK-NEP-1 are highly sensitive, while human neuroblastoma NGP cell line are much less responsive to VEGF blockade therapy (Huang, Frischer 2003, Kim, Serur 2002, Rowe, Huang 2000, Rowe, Huang 2000), likely due to upregulation of alternate proangiogenic pathways. For these experiments, intrarenally implanted xenograft tumors were monitored for growth and randomly assigned to biweekly injections of anti-VEGF antibody BV or vehicle.

Cohorts of tumor-bearing animals were serially imaged at day 0 (pretreatment), and days 1, 3, and 5 after the first drug injection using a high-frequency ultrasound imaging system (Vevo 770, Visualsonics, Toronto, Ontario, Canada) equipped with a 30-MHz transducer. 2D B-mode ultrasound images were acquired using a field of view of 17×17 mm^2. To confirm the characterization of responsiveness, 2D tumor area by ultrasonography was measured using VisualSonics imaging software. The mouse and ultrasound transducer were oriented in the same position between imaging sessions. 2D tumor area was measured in the midsection of the tumor, where the cross-sectional area was the largest. Tumor images from the previous imaging session were used to maximize the accuracy of locating the same 2D plane in each tumor for the duration of the study.

Contrast Enhanced Ultrasound Imaging

CEUS was performed during each imaging session and prior to BV treatment (on days 0 and 3). Mice were anesthetized and tail veins catheterized for injections, as previously described (Sirsi, Feshitan 2010). A 50-μL bolus (2.5×10^7 microbubbles) was injected by hand (~3 sec) followed by a 15-μL saline flush. The bolus was injected while imaging in contrast mode at the maximum frame rate for respiratory gating (~11 frames/second), 100% power. Pilot studies on imaging targeted microbubbles bound to the tumor vasculature demonstrated negligible signal loss until a lower frequency, higher intensity burst pulse was applied, indicating that microbubbles remained stable during normal CEUS imaging. RAD- and RGD-microbubble injections were randomized. Background reference subtraction was performed to detect video intensity enhancement caused by the microbubbles using Visualsonics contrast detection software.

Quantifying Relative Blood Volume

Contrast enhanced ultrasound imaging was performed to evaluate the relative blood volume of the tumors using 2D maximum intensity persistence (MIP) images of the microbubble

contrast enhancement. MIPs were acquired using non-targeted RAD-microbubbles. A region of interest (ROI) was drawn around the hypoechoic tumor region, and the total contrast enhancement was determined by calculating the sum of the linearized pixel intensities within the ROI. A time-intensity curve was generated from the series of MIP images and used to quantify the contrast enhancement. The rationale for using time-intensity curves from the MIP images rather than conventional, frame-by-frame time-intensity curves was based on previous research demonstrating that the maximum enhancement using MIP analysis can capture anti-angiogenic therapy effects more reliably and earlier than conventional time-intensity analysis (Palmowski, Lederle 2009). The relative blood volume was determined from the overall increase in signal intensity of the resulting MIP time-intensity curves. The maximum signal enhancement was calculated by fitting the MIP time-intensity curves to the following equation using the Visualsonics contrast-mode software package:

$$I(t)=A(1-e^{\dagger}(-B*t)) \quad (1)$$

Where I is the linearized video signal intensity, A is the maximum signal enhancement in the ROI, and B is a rate constant describing the influx of contrast agent into the ROI. The relative blood volume (*rbv)* was given as the maximum signal enhancement, A. Equation 1 was used solely to extract the plateau value of the MIP time-intensity curve. The rate constant, B, was not used for data analysis in this study.

Quantifying Relative Targeted Microbubble Adhesion

For ultrasound molecular imaging, a series of proprietary lower frequency, higher pressure burst pulses was applied to destroy microbubbles in the field of view after a 10-minute dwell period (Dayton and Rychak 2007). Video images were captured immediately before and after the microbubble burst pulse, which was implemented through the Visualsonics contrast-mode software package. An ROI was drawn around the hypoechoic tumor region, as above. The contrast enhancement was determined by calculating the sum of the linearized pixel intensities within the ROI. Relative targeted microbubble adhesion (*rtma*) was measured as the difference in video intensity within the ROI for targeted RGD-microbubbles minus that for RAD-microbubbles, as follows:

$$rtma=(\bar{I}_{RGD_{before}}-\bar{I}_{RGD_{after}})-(\bar{I}_{RAD_{before}}-\bar{I}_{RAD_{after}}) \quad (2)$$

where $\bar{I}_{RGD_{before}}$ and $\bar{I}_{RGD_{after}}$ are the average video intensities before and after the burst pulse from the RGD-microbubbles, and $\bar{I}_{RAD_{before}}$ and $\bar{I}_{RAD_{after}}$ are the average video intensities before and after the burst pulse from the RAD-microbubbles. Averages were taken over a 10 second period before and after the burst pulse.

Lectin Perfusion Studies

A portion of mice were sacrificed for microscopic analysis of the tumors. These mice were given identical BV treatment, however CEUS was not performed. At euthanasia, mice were injected with fluorescein-labeled *Lycopersicon esculentum* lectin (100μg/100μL PBS, Vector Laboratories, Burlingame, CA). Vasculature was fixed by infusing 1% paraformaldehyde. 40-μm sections were cut using a vibratome. Computer-assisted image analysis was used to examine changes in specific vessel features by skeletonizing images and then scoring these by computer using Adobe Photoshop 5.0 (Adobe Systems, NY) as described by Wild et al (Wild, Ramakrishnan 2000). Briefly, skeletonizing was performed by converting color images to black and white using a constant threshold value. Black and white images were filtered to remove erroneous spots (non-vessels), then a skeletonization

command (Photoshop) was applied to reduce the vessels to single lines (pixel width of 1) from which the vessel length and number of branching points were determined. 4–8 tumors for each condition (day 0,1,3,5 +/− BV) were examined with 10–15 images per tumor analyzed for vessel length and branching. Histology sections were taken in random sections of the tumor.

Statistical methods

For the blood volume measurements, a linear mixed effects regression model was implemented using the SAS PROC MIXED procedure (SAS Software Version 9.1, SAS Institute, Cary, NC) to evaluate differences in overall trends between cohorts. The model estimates linear trajectories for each cohort over time, while accounting for comparisons among repeated measurements from the same mice. The intercept was treated as a random effect and covariate to account for the differences between mice at baseline. A maximum likelihood method was used for estimation of the regression coefficient. For the ultrasound targeted imaging, a non-linear model was implemented using the SAS PROC NLMIXED procedure including random effects. A non-linear model was required for *rtma* measurements since the data was constrained by a lower limit (0% of initial binding), which several mice reached 3 days following treatment. The data was then fit to an exponential decay (e^{-kt}). The decay constant (k) term was used for comparison between cohorts. Comparisons of lectin perfusion studies, as well as relative changes in mean tumor size, *rbv,* and *rtma* values, between BV- and vehicle-treated and day 0 control tumors at days 1, 3, and 5 were calculated using a two-tailed parametric Student's t-test.

Results

Microbubble Size Distribution

Figure 1 shows typical number and volume weighted size distributions for the microbubbles used in this study. The number-weighted median diameter was 4.5 ± 0.7 μm, which is slightly smaller than the diameter of a typical red blood cell. A small portion of microbubbles greater than 8 μm (~7%) were present, which may have been larger than some neovessels in the tumor. However, we recently showed that similar size distributions showed insignificant trapping in the renal vasculature of healthy mice (Sirsi, Hernandez 2011), indicating that larger microbubbles can deform or dissolve to accommodate vessel constrictions, as was previously observed by Lindner et al. for Definity® microbubbles (Lindner, Song 2002).

Tumor Size Progression

Tumor progression was monitored by ultrasonography as hypoechoic areas in the B-mode images (Fig 2). Treatment of SK-NEP-1 mice with BV essentially arrested tumor growth over the 5 day period (4.7 ± 8.6% mean decrease in cross-sectional area), compared with continued growth in the control tumors (41.7 ± 28.4% mean increase in cross-sectional area) ($P<0.05$). Growth of NGP tumors was unaffected by BV treatment (44.1 ± 31.4% vs. 97.3 ± 96.9%, BV vs. control, $P=0.28$). These results along with analysis of lectin perfusion studies of the vasculature (see *Lectin Perfusion* results), verify our classification of SK-NEP-1 as a responder and NGP as a non-responder to VEGF blockade therapy.

Relative Blood Volume

The relative blood volume (*rbv*) of the tumor was measured using the total microbubble signal enhancement. The *rbv* in SK-NEP-1 and NGP xenograft tumors was measured using high-frequency ultrasound and size-selected microbubbles optimized for CEUS imaging studies. Figure 3 shows representative CEUS images with contrast overlays (green) for

control and BV treated SK-NEP-1 (Fig. 3A) and NGP mice (Fig. 3B) before and 3 days after treatment. The hypoechoic tumor regions are outlined in white. Following microbubble injection, contrast was observed heterogeneously throughout the tumor region. In some cases for SK-NEP-1 control and NGP treated/control, the tumor midsection grew such that the periphery was outside the 17×17 mm^2 field of view by day 5. This was not observed for BV-treated SK-NEP-1 tumors.

Figure 4 shows results for *rbv* for the four groups. The *rbv* showed no trend in the individual BV-treated SK-NEP-1 mice (Fig. 4A), while an increasing trend was observed in BV-treated NGP tumors (Fig. 4B), indicating that NGP tumors were unresponsive to BV therapy. The mean *rbv* in BV-treated SK-NEP-1 tumors was unchanged at days 1, 3 and 5 (P=0.67, 0.66 and 0.40, respectively) (Fig. 4C). BV-treated NGP tumors, on the other hand, showed an increase in mean *rbv* of 38±21% (P=0.0004) by day 1, 57±48% (P=0.0056) by day 3 and 105±41% (P<0.00001) by day 5 (Fig. 4D). For the control groups, mean *rbv* increased for both SK-NEP-1 and NGP tumors by day 5 (P=0.034 and 0.0096, respectively). A linear mixed-effects model was used to evaluate the combined effects over 5 days (Fig. 4C,D). The slopes of the linear regression between BV-treated and control SK-NEP-1 cohorts were statistically different (P=0.0044), while no difference between the NGP treated and control group was observed (P=0.25). Thus, CEUS imaging showed that BV treatment arrested the increase in microbubble signal intensity in responder SK-NEP-1 tumors, but not the other groups.

Relative Targeted Microbubble Adhesion

CEUS imaging using targeted microbubbles was used to evaluate $\alpha_V\beta_3$ integrin, which is expressed preferentially on actively proliferating vessels found in growing tumors (Brooks, Clark 1994). Microbubbles were targeted to this epitope by surface conjugation of RGD peptide (RAD peptide serving as control). Figure 5 shows representative CEUS images with contrast overlays (green) for BV-treated SK-NEP-1 (Fig. 5A) and NGP mice (Fig. 5B) before and 3 days after treatment. Images are shown before and after a burst pulse (BP) was applied to destroy targeted microbubbles bound to the angiogenic vasculature. Time-intensity curves over this period are also shown.

Relative targeted microbubble adhesion (*rtma*) was quantified by the drop in tumor pixel intensity following the microbubble-burst pulse (*versus* RAD control) (Fig. 6). For SK-NEP-1 tumors, all BV-treated mice showed a significant reduction in *rtma* values by day 3 (Fig. 6A). No trend was observed for BV-treated NGP tumors (Fig. 6B). BV-treated SK-NEP-1 mean *rtma* did not change significantly after 1 day, but it decreased 91±5% (P<0.00001) by day 3 and 99±5% (P<0.00001) by day 5 (Fig. 6C). The mean *rtma* values decreased also for BV-treated NGP and control mice, but at slower rates (Fig. 5D). The decay rates were compared using a non-linear exponential decay model (Fig. 6C,D). The difference in decay rates between BV-treated and control SK-NEP-1 were statistically different (P=0.022), while no difference was observed between treated and control NGP (P=0.26). Thus, ultrasound molecular imaging showed a robust decrease in $\alpha_V\beta_3$ integrin expression as early as 3 days following BV treatment only for the responder, SK-NEP-1, and not the other groups.

Lectin Perfusion

Quantified changes in lectin perfusion studies of tumor vasculature were consistent with changes detected by CEUS. As compared to day 0 controls, microvessel density (MVD) in BV-treated SK-NEP-1 tumors decreased by 66% at day 1, 75% at day 3, and 78% at day 5 (P=0.003, each), whereas MVD did not change in BV-treated NGP tumors. Control SK-NEP-1 and NGP tumor perfusion also did not change over the experimental period. BV

treatment significantly decreased total vessel length in SK-NEP-1 at days 1, 3, 5 (P=0.01, P=0.01, P=0.001), but not in NGP tumors (Fig. 7b). New vascular branches can form a dynamic and relatively VEGF-dependent element in angiogenic networks. Similar to the pattern of change detected in the $\alpha_V\beta_3$ integrin-expressing vessels using RGD-tagged microbubbles, BV significantly decreased total vascular branch number in SK-NEP-1 at days 3 and 5 (P=0.014), but not in NGP (Fig. 7c). A small but significant increase in vessel length and branching is observed in NGP control tumors at Day 1 only ($P<0.05$), however no overall trend is observed over the course of 5 days. Taken together, these analyses suggest that BV treatment reduced overall perfusion in SK-NEP-1 tumors, with disproportionate pruning of smaller, branch vessels.

Discussion

Biologically targeted agents hold promise for increasing effectiveness of cancer treatment, yet optimizing their use may require the development of new assessment strategies. In this set of preclinical studies, we have demonstrated that it is possible to clearly distinguish responder from non-responder tumors after BV treatment in cohorts of mice, sometimes as early as 3 days after treatment initiation. Prognostic imaging biomarkers, including tumor size progression, total microbubble signal enhancement (proportional to blood volume), and relative targeted microbubble adhesion (proportional to $\alpha_V\beta_3$ integrin concentration on the luminal surface of the endothelium) were identified using CEUS. The techniques used in the study and the corresponding results are critically analyzed below and compared to suggest possible prognostic methods of evaluating tumor responses to BV therapy.

Tumor size progression

Tumor growth was assessed using 2D ultrasonography in order to measure increases in tumor area. BV treated SK-NEP-1 tumors did not statistically change in size during the experiment after administration of BV treatment (Fig. 2). Lack of tumor regression is consistent with previous studies on the effects of anti-angiogenic therapy in similar tumor models (Guibal, Taillade 2010, Pysz, Foygel 2010). Overall, control or unresponsive tumors grew rapidly, increasing in cross-sectional area ranging up to 100% in 5 days after initiating treatment. Previous research on BV treatment in similar SK-NEP-1 tumor models indicates that untreated tumors grew 3–4 weeks before their tumor areas increased to the same degree observed in this study (Guibal, Taillade 2010). The rapid growth observed in these prior studies may be attributed to different stages of tumor growth before initiating BV treatment (initial tumor sizes were not reported by Guibal et al.). The change in tumor morphology over the course of the experiment may be a potential source of error for 2D image analysis, given the increased difficulty in identifying the exact portion of the tumor that was previously imaged. However, we were able detect significant increases in tumor area 5 days after initiating BV treatment, indicating that our methodology for monitoring tumor progression was adequate. The tumor progression rates observed in this study may be atypical compared to those observed in clinical practice, thus we do not expect that monitoring tumor progression by changes in cross-sectional area alone is an adequate approach for monitoring BV therapy.

Relative Blood Volume

The *rbv* in tumors was measured by the total contrast enhancement within the hypoechoic tumor region caused by bolus injections of microbubbles. The total contrast enhancement was measured, as opposed to mean contrast enhancement per area, to account for variability in tumor perfusion during tumor growth. SK-NEP-1 tumors exhibit necrosis during tumor progression (Guibal, Taillade 2010), which decreases the mean blood volume, and therefore changes in total signal enhancement are a more appropriate measure of changes in the total

blood volume. The *rbv* represents one of the simplest methods of measuring a basic parameter related to the tumor vasculature that could be applied in a clinical setting.

BV treated SK-NEP-1 tumors showed a slight decrease in *rbv* while SK-NEP-1 control and NGP tumors all showed increased *rbv* levels (Fig. 3). Interestingly, histology indicates that BV treated SK-NEP-1 tumors exhibit reduced vessel lengths and fewer vessel branching points detectable one day following BV treatment (Fig. 7). Based on the histological results, one would expect that *rbv* levels should be much lower in BV treated SK-NEP-1 tumors. This suggests that the overall blood volume measured by our CEUS methodology may be skewed towards detecting larger established vessels that are minimally affected by BV treatment. Additionally, changes in morphology during tumor progression may be responsible for the variability in *rbv* values observed during longitudinal imaging. It is likely that the sensitivity of the *rbv* parameter would benefit from nonlinear contrast modes and 3D ultrasonography to measure microbubble signal in the tumor volumes (Feingold, Gessner 2010). Overall, CEUS imaging of the *rbv* shows a difference in trends between BV treated and control SK-NEP-1 cohorts.

Relative Targeted Microbubble Adhesion

The *rtma* parameter was a more consistent predictor of response compared to the *rbv.* BV treated SK-NEP-1 tumors showed significant decreases in *rtma* by day 3, with 100% of treated mice exhibiting less than 15% of their initial *rtma* values. The mean *rtma* value 1 day after initiating BV treatment was slightly lower (87 ± 59% of pre-treatment *rtma*), consistent with the histological analysis of tissue, although this was not statistically significant compared to the pre-treatment *rtma* (P=0.61, Fig. 6C). The results observed in this study are consistent with previous research demonstrating a significant reduction in targeted microbubble binding after initiating anti-angiogenic therapy in LS174T colon cancer xenografts (Pysz, Foygel 2010). These results also are consistent with the histological findings presented here and similar studies described previously (Bagi and Anderson 2010, Hudson, Williams 2011, Mancuso, Davis 2006, Watson, Hu 2011).

The *rtma* analysis demonstrates lower levels of targeted microbubble binding in NGP tumors prior to treatment. This may be due to variability in endogenous levels of $\alpha_V\beta_3$ integrin expression between the two tumor models; however, this has yet to be confirmed histologically. A low initial level of targeted microbubble binding reduces the sensitivity of the measurement and may cause false positive results in predicting BV tumor response. We also observed a small degree of nonspecific binding for the RAD control microbubbles in SK-NEP-1 at baseline (Fig. 5A). This result indicates that nonspecific adhesion was more prevalent in the neovasculature (i.e., short branches), which were reduced by the BV treatment. Improving molecular imaging sensitivity therefore may be necessary for clinical application. This could be accomplished by varying targeted microbubble dosages, improving ligand specificity, or application of acoustic radiation forces during imaging to promote microbubble-ligand interactions (Rychak, Klibanov 2007, Zhao, Borden 2004).

Decreases in *rtma* were observed unexpectedly for SK-NEP-1 control and NGP tumors over the course of 5 days. The reduced *rtma* is inconsistent with histological evidence, which shows no effect on the vasculature in these groups. One possible explanation is that the decrease in *rtma* is an artifact of 2D ultrasonography in combination with rapid tumor progression (Feingold, Gessner 2010). More vascularized portions of the tumor are likely moving out of the 2D field of view during tumor progression, artificially reducing the *rtma* value. As with measuring *rbv*, the *rtma* measurements would likely benefit from 3D ultrasonography to measure microbubble binding in the entire tumor volume. Despite some false positive errors that were observed in SKNEP control and NGP tumors, molecular imaging of $\alpha_V\beta_3$ shows promise towards discerning responders and non-responders.

Conclusion

Overall, our study suggests that development of rapid, imaging-based assessments for human patients is feasible. Molecular imaging techniques may be a more robust predictor of BV response compared to perfusion imaging. However, future double-blind, long-term studies with improved imaging methodology (e.g., nonlinear contrast modes and 3D) are necessary to determine the efficacy for accurately predicting individual tumor responses. Future work should also focus on the relation to biological consequences, such as changes in vascular permeability, metastatic potential, hypoxia and other indicators of vascular remodeling. With such improvements, the development of microbubbles targeted to cancer endothelial biomarkers could make this technology a first-line modality for diagnosing and monitoring cancer angiogenesis, and molecular ultrasound imaging as demonstrated here is a step toward individualized medicine. Coordinated clinical use of such data could provide significant benefits for patients by enabling earlier and more effective clinical decision-making. Lastly, given the high cost of biologically targeted therapies like BV, such early assessment of drug effectiveness could reduce the economic strains of cancer treatment for patients and families.

References

Bagi CM, Anderson CD. Models of hepatocellular carcinoma and biomarker strategy. Cancers. 2010; 2:1441–52.

Brooks PC, Clark RA, Cheresh DA. Requirement of vascular integrin alpha v beta 3 for angiogenesis. Science. 1994; 264:569–71. [PubMed: 7512751]

Cheung AM, Brown AS, Cucevic V, Roy M, Needles A, Yang V, Hicklin DJ, Kerbel RS, Foster FS. Detecting vascular changes in tumour xenografts using micro-ultrasound and micro-ct following treatment with VEGFR-2 blocking antibodies. Ultrasound Med Biol. 2007; 33:1259–68. [PubMed: 17467156]

Dayton PA, Rychak JJ. Molecular ultrasound imaging using microbubble contrast agents. Front Biosci. 2007; 12:5124–42. [PubMed: 17569635]

Feingold S, Gessner R, Guracar IM, Dayton PA. Quantitative volumetric perfusion mapping of the microvasculature using contrast ultrasound. Investigative Radiology. 2010; 45:669–74. [PubMed: 20808232]

Feshitan JA, Chen CC, Kwan JJ, Borden MA. Microbubble size isolation by differential centrifugation. J Colloid Interface Sci. 2009; 329:316–24. [PubMed: 18950786]

Forsberg F, Ro RJ, Potoczek M, Liu JB, Merritt CR, James KM, Dicker AP, Nazarian LN. Assessment of angiogenesis: implications for ultrasound imaging. Ultrasonics. 2004; 42:325–30. [PubMed: 15047306]

Guibal A, Taillade L, Mule S, Comperat E, Badachi Y, Golmard JL, Le Guillou-Buffello D, Rixe O, Bridal SL, Lucidarme O. Noninvasive contrast-enhanced US quantitative assessment of tumor microcirculation in a murine model: effect of discontinuing anti-VEGF therapy. Radiology. 2010; 254:420–9. [PubMed: 20093514]

Hoyt K, Warram JM, Umphrey H, Belt L, Lockhart ME, Robbin ML, Zinn KR. Determination of breast cancer response to bevacizumab therapy using contrast-enhanced ultrasound and artificial neural networks. Journal of Ultrasound in Medicine. 2010; 29:577–85. [PubMed: 20375376]

Huang J, Frischer JS, Serur A, Kadenhe A, Yokoi A, McCrudden KW, New T, O'Toole K, Zabski S, Rudge JS, Holash J, Yancopoulos GD, Yamashiro DJ, Kandel JJ. Regression of established tumors and metastases by potent vascular endothelial growth factor blockade. Proc Natl Acad Sci U S A. 2003; 100:7785–90. [PubMed: 12805568]

Hudson JM, Williams R, Lloyd B, Atri M, Kim TK, Bjarnason G, Burns PN. Improved flow measurement using microbubble contrast agents and disruption-repleneshment: clinical application to tumour monitoring. Ultrasound Med Biol. 2011; 37:1210–21. [PubMed: 21683508]

Kim ES, Serur A, Huang J, Manley CA, McCrudden KW, Frischer JS, Soffer SZ, Ring L, New T, Zabski S, Rudge JS, Holash J, Yancopoulos GD, Kandel JJ, Yamashiro DJ. Potent VEGF

blockade causes regression of coopted vessels in a model of neuroblastoma. Proc Natl Acad Sci U S A. 2002; 99:11399–404. [PubMed: 12177446]

Lamuraglia M, Escudier B, Chami L, Schwartz B, Leclere J, Roche A, Lassau N. To predict progression-free survival and overall survival in metastatic renal cancer treated with sorafenib: pilot study using dynamic contrast-enhanced Doppler ultrasound. Eur J Cancer. 2006; 42:2472–9. [PubMed: 16965911]

Lassau N, Lamuraglia M, Chami L, Leclere J, Bonvalot S, Terrier P, Roche A, Le Cesne A. Gastrointestinal stromal tumors treated with imatinib: monitoring response with contrast-enhanced sonography. AJR Am J Roentgenol. 2006; 187:1267–73. [PubMed: 17056915]

Lindner JR, Song J, Jayaweera AR, Sklenar J, Kaul S. Microvascular rheology of definity microbubbles after intra-arterial and intravenous administration. Journal of the American Society of Echocardiography. 2002; 15:396–403. [PubMed: 12019422]

Mancuso MR, Davis R, Norberg SM, O'Brien S, Sennino B, Nakahara T, Yao VJ, Inai T, Brooks P, Freimark B, Shalinsky DR, Hu-Lowe DD, McDonald DM. Rapid vascular regrowth in tumors after reversal of VEGF inhibition. Journal of Clinical Investigation. 2006; 116:2610–21. [PubMed: 17016557]

Palmowski M, Lederle W, Gaetjens J, Socher M, Hauff P, Bzyl J, Semmler W, Gunther RW, Kiessling F. Comparison of conventional time-intensity curves vs. maximum intensity over time for post-processing of dynamic contrast-enhanced ultrasound. Eur J Radiol. 2009; 75:e149–53. [PubMed: 19945241]

Pysz MA, Foygel K, Rosenberg J, Gambhir SS, Schneider M, Willmann JK. Antiangiogenic Cancer Therapy: Monitoring with Molecular US a Clinically Translatable Contrast Agent (BR55). Radiology. 2010; 256:519–27. [PubMed: 20515975]

Rowe DH, Huang J, Kayton ML, Thompson R, Troxel A, O'Toole KM, Yamashiro D, Stolar CJ, Kandel JJ. Anti-VEGF antibody suppresses primary tumor growth and metastasis in an experimental model of Wilms' tumor. J Pediatr Surg. 2000; 35:30–2. discussion 32-3. [PubMed: 10646769]

Rowe DH, Huang J, Li J, Manley C, O'Toole KM, Stolar CJ, Yamashiro DJ, Kandel JJ. Suppression of primary tumor growth in a mouse model of human neuroblastoma. J Pediatr Surg. 2000; 35:977–81. [PubMed: 10873048]

Rychak JJ, Klibanov AL, Ley KF, Hossack JA. Enhanced targeting of ultrasound contrast agents using acoustic radiation force. Ultrasound Med Biol. 2007; 33:1132–9. [PubMed: 17445966]

Sirsi S, Feshitan J, Kwan J, Homma S, Borden M. Effect of microbubble size on fundamental mode high frequency ultrasound imaging in mice. Ultrasound Med Biol. 2010; 36:935–48. [PubMed: 20447755]

Sirsi SR, Hernandez SL, Zielinski L, Blomback H, Koubaa A, Synder M, Homma S, Kandel J, Yamashiro DY, Borden MA. Polyplex-microbubble hybrids for ultrasound-guided plasmid DNA delivery to solid tumors. J Control Release. 2011 in press.

Smith MA, Morton CL, Phelps D, Girtman K, Neale G, Houghton PJ. SK-NEP-1 and Rh1 are Ewing family tumor lines. Pediatric blood & cancer. 2008; 50:703–6. [PubMed: 17154184]

Streeter JE, Gessner R, Miles I, Dayton PA. Improving sensitivity in ultrasound molecular imaging by tailoring contrast agent size distribution: in vivo studies. Mol Imaging. 2010; 9:87–95. [PubMed: 20236606]

Unger E, Lund P, Shen D, Fritz T, Yellowhair D, New T. Nitrogen-filled liposomes as a vascular US contrast agent: preliminary evaluation. Radiology. 1992; 185:453–56. [PubMed: 1410353]

Watson KD, Hu X, Lai CY, Lindfors HA, Hu-Lowe DD, Tuthill TA, Shalinsky DR, Ferrara KW. Novel ultrasound and DCE-MRI analyses after antiangiogenic treatment with a selective VEGF receptor inhibitor. Ultrasound Med Biol. 2011; 37:909–21. [PubMed: 21531499]

Wild R, Ramakrishnan S, Sedgewick J, Griffioen AW. Quantitative assessment of angiogenesis and tumor vessel architecture by computer-assisted digital image analysis: effects of VEGF-toxin conjugate on tumor microvessel density. Microvasc Res. 2000; 59:368–76. [PubMed: 10792968]

Williams R, Hudson JM, Lloyd BA, Sureshkumar AR, Lueck G, Milot L, Atri M, Bjarnason GA, Burns PN. Dynamic Microbubble Contrast-enhanced US to Measure Tumor Response to Targeted

Therapy: A Proposed Clinical Protocol with Results from Renal Cell Carcinoma Patients Receiving Antiangiogenic Therapy. Radiology. 2011; 260:581–90. [PubMed: 21555352]

Wilson SR, Burns PN. Microbubble-enhanced US in body imaging: what role? Radiology. 2010; 257:24–39. [PubMed: 20851938]

Wilson SR, Greenbaum LD, Goldberg BB. Contrast-Enhanced Ultrasound: What Is the Evidence and What Are the Obstacles? Am J Roentgenol. 2009; 193:55–60. [PubMed: 19542395]

Zhao S, Borden M, Bloch SH, Kruse D, Ferrara KW, Dayton PA. Radiation-force assisted targeting facilitates ultrasonic molecular imaging. Mol Imaging. 2004; 3:135–48. [PubMed: 15530249]

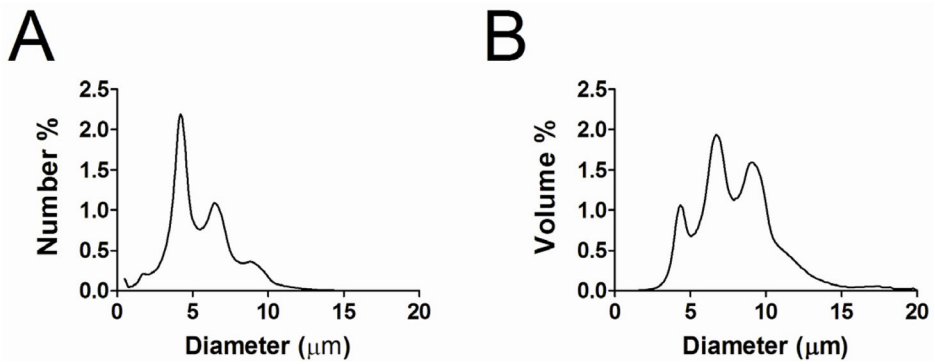

Figure 1.
Typical number-weighted (A) and volume-weighted (B) distributions of size-selected microbubbles after removal of the sub-2 μm diameter population.

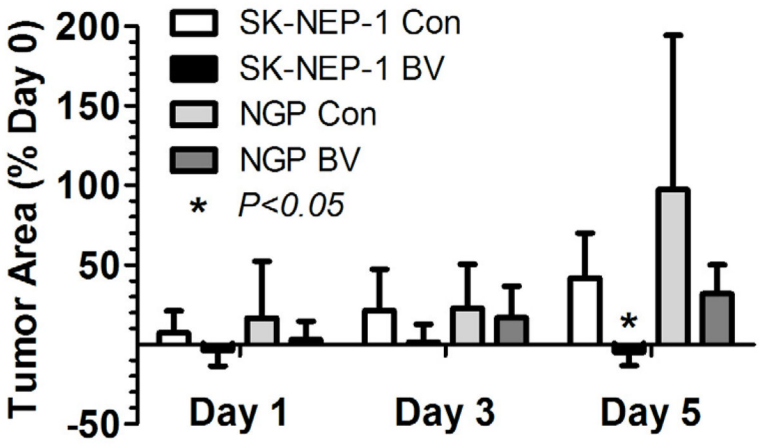

Figure 2.

Bevacizumab arrests tumor growth in SK-NEP-1 tumors but not NGP tumors. NCR Nude mice implanted with either SK-NEP-1 or NGP renal tumors were imaged with high-frequency ultrasound following bolus injections of size-selected microbubbles. Mice were imaged at 0, 1, 3, and 5 days. Bevacizumab (BV) or albumin (Con) was administered immediately after the imaging sessions on days 0 and 3. The tumor 2D cross-sectional area was determined from the ultrasound images using Visualsonics software. Area measurements of the tumor were calculated from the ultrasound images using a region of interest (ROI) that encompassed the hypoechoic region of the kidney (tumor tissue). All area measurements were performed in the midsection of the tumor. The tumor areas for BV-treated and Con groups were compared for the SK-NEP-1 (n=6 and 7, respectively) and NGP cohorts (n=7 and 7, respectively). BV treatment significantly arrested tumor growth in SK-NEP-1 xenografts at day 5 in comparison to control, but not in NGP xenografts, *$p<0.05$ relative to albumin control (Con).

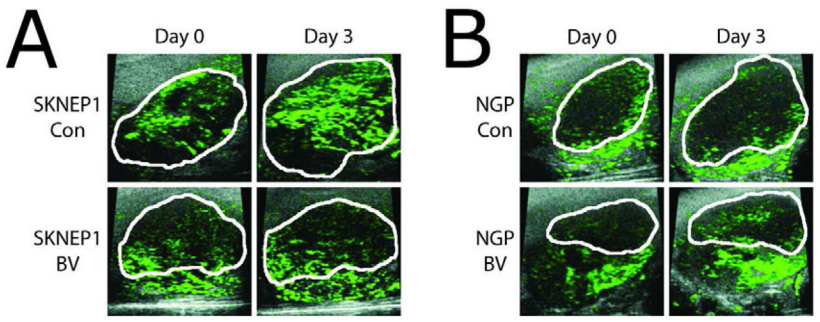

Figure 3.

CEUS images of relative tumor blood volume measured by microbubble signal enhancement. Representative tumors with total microbubble signal enhancement overlays from the (A) SK-NEP-1 and (B) NGP groups are shown at day 0 and day 3. Hypoechoic tumor regions are outlined in white and microbubble signal enhancement is colored green. In contrast to the SK-NEP-1 Con, NGP Con, and NGP BV groups, the BV-treated SK-NEP-1 tumors showed no increase in size or microbubble signal enhancement. The field of view for each of the ultrasound images was 17×17 mm^2.

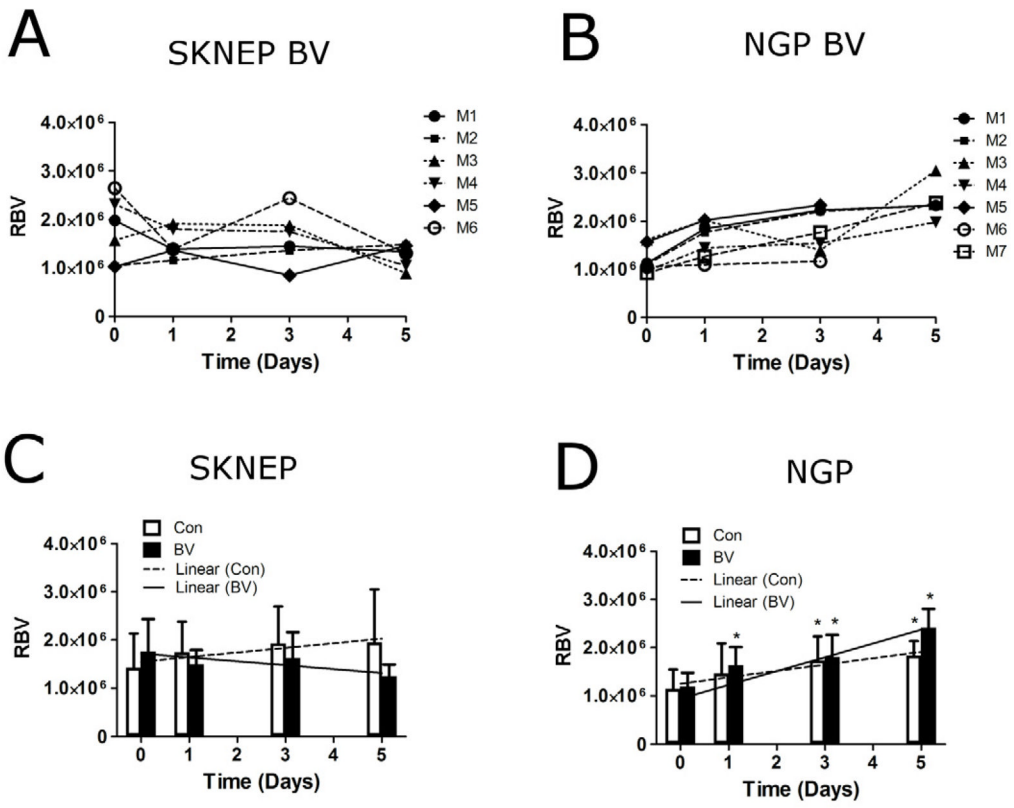

Figure 4.

CEUS evaluation of tumor blood volume. The relative blood volume (*rbv*) was quantified in the tumor region on days 0, 1, 3, and 5. (A) Individual BV-treated SK-NEP-1 tumors show no overall trend over 5 days, whereas (B) a noticeable increase in *rbv* is observed for BV-treated NGP mice. Mean *rbv* values are shown at each day for (C) SK-NEP-1 and (D) NGP tumors. Linear regression lines were applied to the mean *rbv* values from 0 to 5 days for the Con (---) and BV (—) groups. The slope of the regression lines for Con (□) and BV-treated (■) tumors were compared for the SK-NEP-1 (n=7 and 6, respectively) and NGP cohorts (n=6 and 7, respectively) using a linear mixed-effects model. * indicates that the mean value was significantly different from the initial baseline measurement ($P<0.05$).

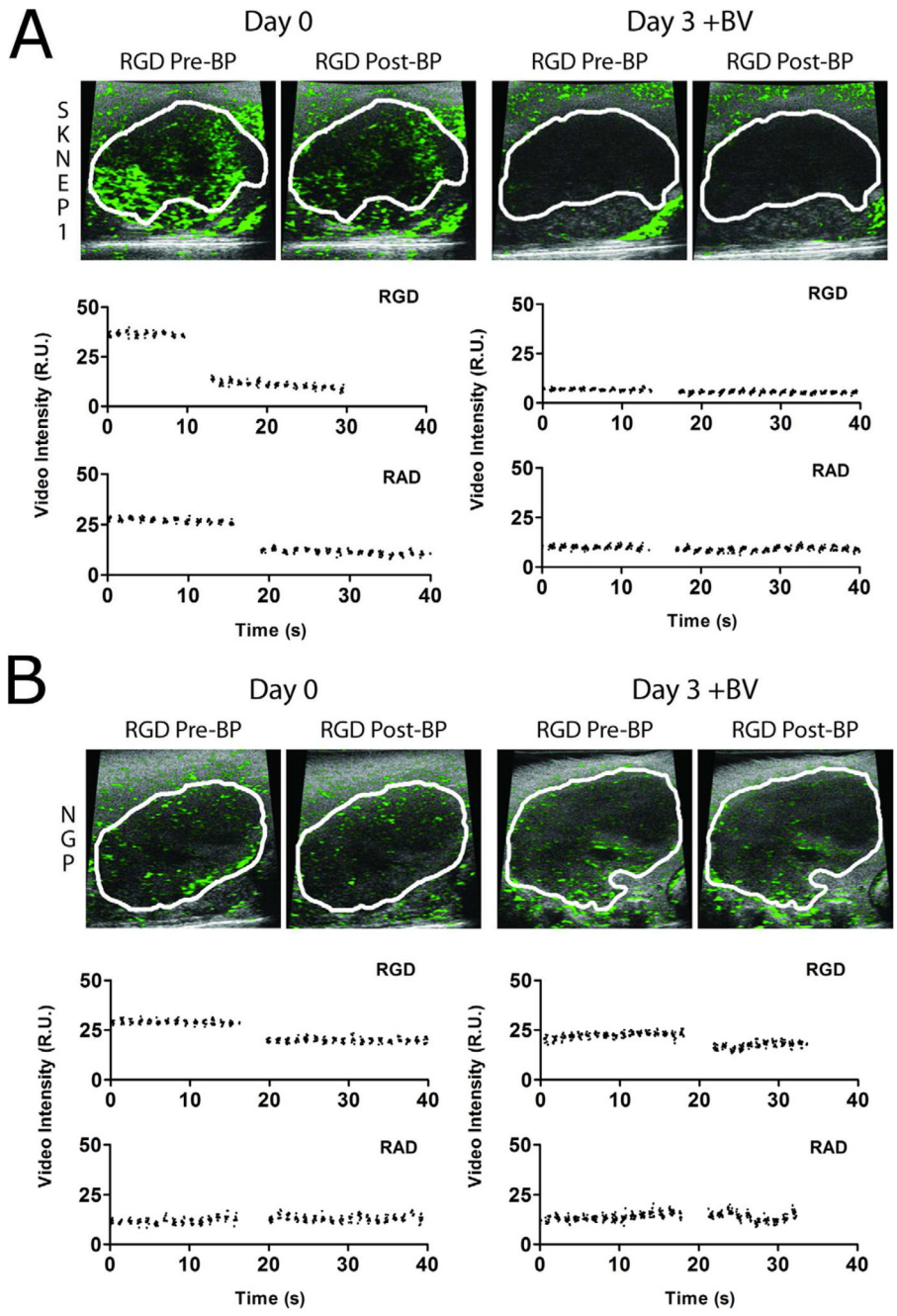

Figure 5.

CEUS images of tumor angiogenesis. The expression of $\alpha_V\beta_3$ integrin in the vessels of the tumor region was evaluated in the same mice using CEUS with RGD-labeled microbubbles (*versus* RAD control). Representative tumors with microbubble contrast overlays from the (A) SK-NEP-1 and (B) NGP groups are shown at day 0 and day 3 following a 10-min dwell time after bolus injection (5×10^8 mL^{-1}, 50 μL). Images are shown before (left) and after (right) the burst pulse was applied to fragment the microbubbles in the field of view. The corresponding video intensity-time curve is shown below each pair of images for both RGD-labeled (blue) and RAD-labeled (red) microbubble injections.

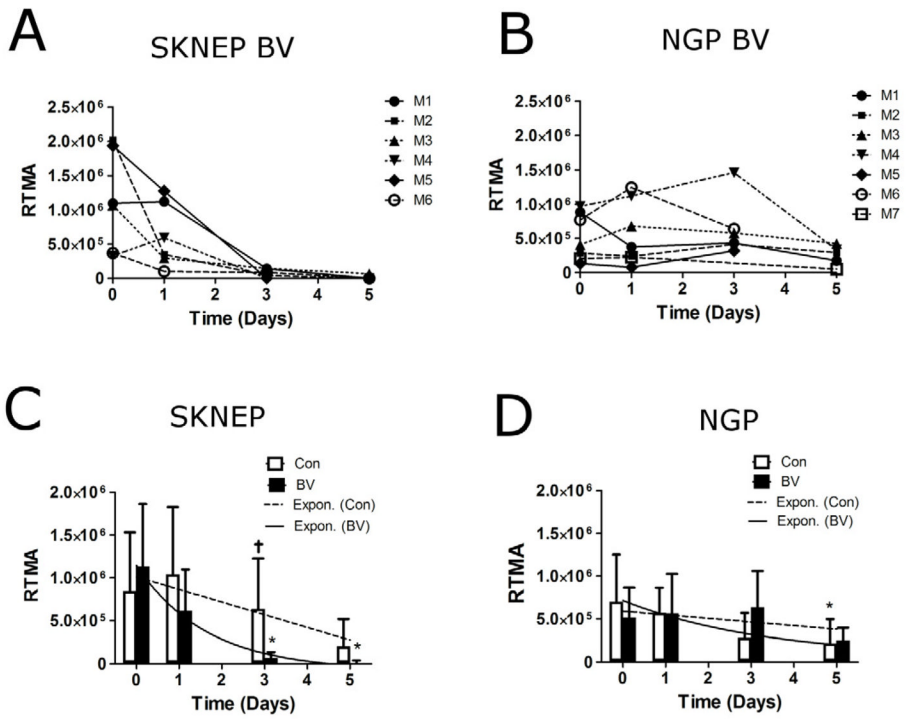

Figure 6.

CEUS evaluation of tumor angiogenesis. The relative targeted microbubble adhesion (*rtma*) was quantified in the tumor region on days 0, 1, 3, and 5. (A) All BV-treated SK-NEP-1 tumors showed a dramatic decrease in *rtma* at day 3, which remained consistently low at day 5. (B) No noticeable trend was observed in BV-treated NGP tumors. Mean *rtma* values are shown for (C) SK-NEP-1 and (D) NGP tumors for BV treated and control groups. An exponential curve fit (e^{-kt}) was applied to the Con (---) and BV (—) groups using a non-linear mixed-effects model. The decay constant (k) for Con (□) and BV-treated (■) groups were compared for the SK-NEP-1 (n=7 and 6, respectively) and NGP cohorts (n=7 and 7, respectively).

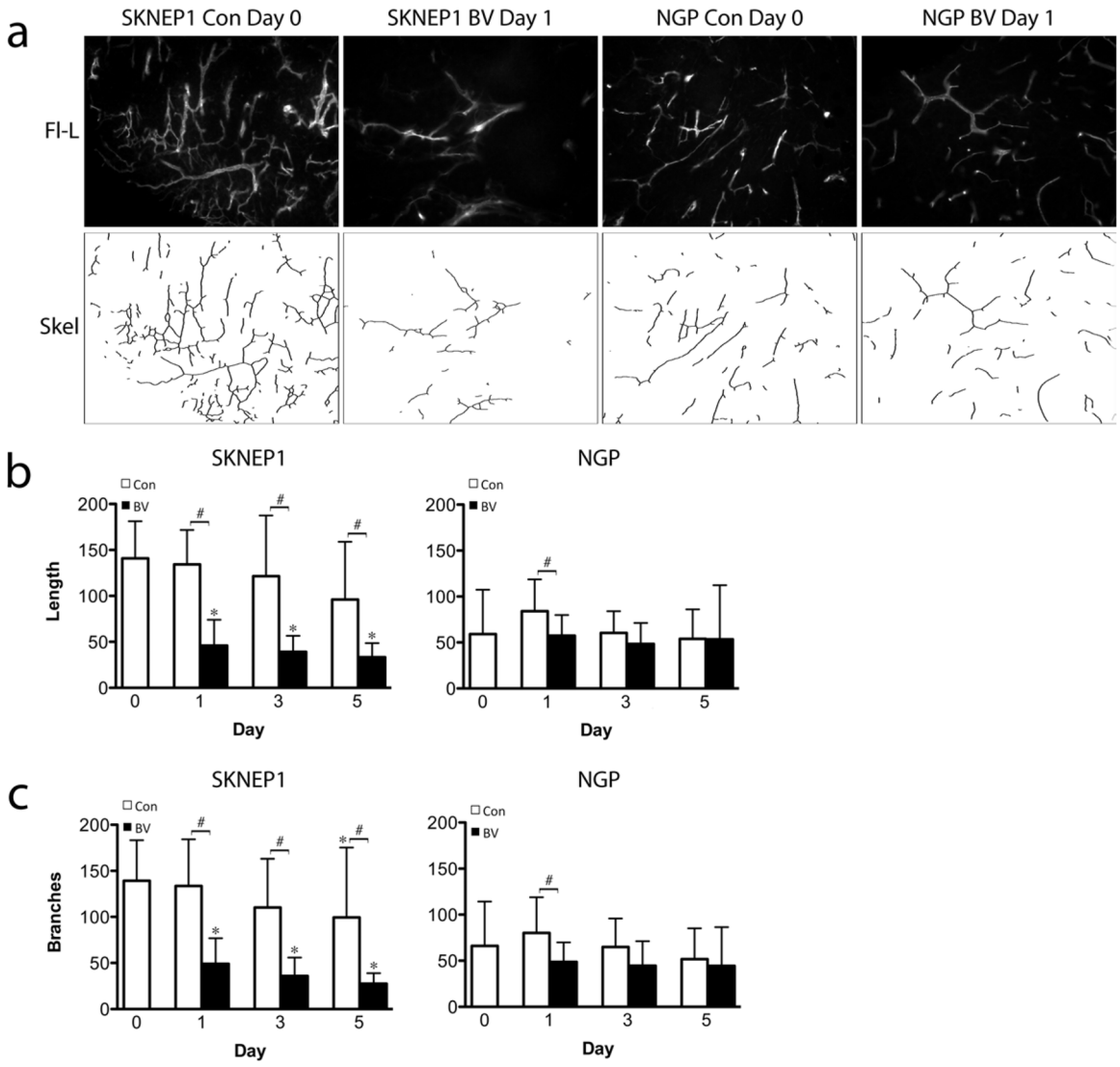

Figure 7.

Established SK-NEP-1 and NGP tumors were injected IV with fluorescein-labeled *L. esculentum* lectin, prior to sacrifice at day 0, or after 1, 3, or 5 days of treatment with either vehicle (Con) or bevacizumab (BV). (A) Representative fluorescent images at days 0 and 3 of BV treatment. After binarization of the images, total length was calculated by skeletonizing the images and then scoring total vessel length (B) and number of branch points (C) by computer. BV treatment significantly decreased vessel length and branching in SK-NEP-1 at days 1, 3, 5 (*$p<0.05$ relative to baseline, #$p<0.05$ relative to control), but not in NGP tumors.